

Electronic Structure of Multilayer Graphene

Hongki MIN^{*)} and Allan H. MACDONALD

Department of Physics, University of Texas at Austin, Austin, Texas 78712, USA

We study the electronic structure of multilayer graphene using a π -orbital continuum model with nearest-neighbor intralayer and interlayer tunneling. Using degenerate state perturbation theory, we show that the low-energy electronic structure of arbitrarily stacked graphene multilayers consists of chiral pseudospin doublets with a conserved chirality sum.

§1. Introduction

The recent explosion^{1),2)} of research on the electronic properties of single layer and stacked multilayer graphene sheets has been driven by advances in material preparation methods,^{3),4)} by the unusual^{5),6),7)} electronic properties of these materials including unusual quantum Hall effects,^{8),9)} and by hopes that these elegantly tunable systems might be useful electronic materials.

In this paper,¹⁰⁾ we study the electronic structure of arbitrarily stacked multilayer graphene using a π -orbital continuum model with only near-neighbor interactions, analyzing its low-energy spectrum using degenerate state perturbation theory. Here we focus solely on aligned multilayer graphene without rotational stacking faults.¹¹⁾ Interestingly, we find that the low-energy effective theory of multilayer graphene is always described by a set of chiral pseudospin doublets with a conserved chirality sum. We discuss implications of this finding for the quantum Hall effect in multilayer graphene.

§2. π -orbital continuum model

We consider the π -orbital continuum model for N -layer graphene Hamiltonian which describes bands near the hexagonal corners of the triangular lattice Brillouin zone, the K and K' points:

$$\mathcal{H} = \sum_{\mathbf{p}} \Psi_{\mathbf{p}}^{\dagger} H(\mathbf{p}) \Psi_{\mathbf{p}}, \quad (2.1)$$

where $\Psi_{\mathbf{p}} = (c_{1,\alpha,\mathbf{p}}, c_{1,\beta,\mathbf{p}}, \dots, c_{N,\alpha,\mathbf{p}}, c_{N,\beta,\mathbf{p}})$ and $c_{l,\mu,\mathbf{p}}$ is an electron annihilation operator for layer $l = 1, \dots, N$, sublattice $\mu = \alpha, \beta$ and momentum \mathbf{p} measured from K or K' point.

The simplest model for a multilayer graphene system allows only nearest-neighbor intralayer hopping t and the nearest-neighbor interlayer hopping t_{\perp} . The in-plane Fermi velocity v is related with t by $\frac{\hbar v}{a} = \frac{\sqrt{3}}{2}t$, where $a = 2.46 \text{ \AA}$ is a lattice constant of monolayer graphene. Although this model is not fully realistic, some aspects of the electronic structure can be understood by fully analyzing the properties of this simplified model first and then considering corrections.

^{*)} E-mail: hongki@physics.utexas.edu

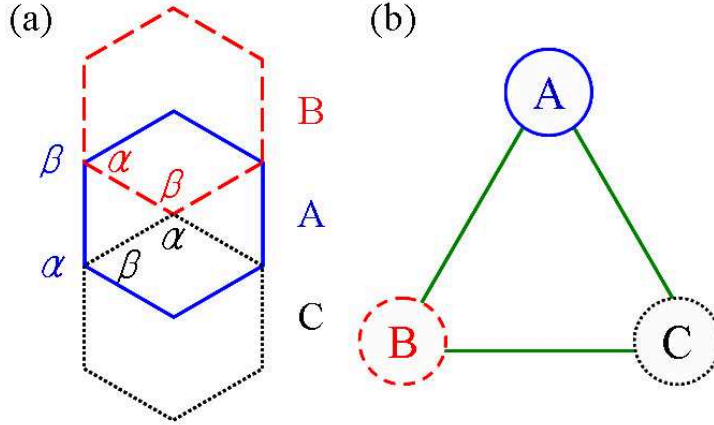


Fig. 1. (Color online) (a) Energetically favored stacking arrangements for graphene sheets. The honeycomb lattice of a single sheet has two triangular sublattices, labeled by α and β . Given a starting graphene sheet, the honeycomb lattice for the next layer is usually positioned by displacing either α or β sublattice carbon atoms along a honeycomb edge. There are therefore in three distinct two-dimensional (2D) sheets, labeled by A, B, and C. Representative α and β sublattice positions in A, B, and C layers are identified in this illustration. It is also possible to transform between layer types by rotating by $\pm 60^\circ$ about a carbon atom on one of the two sublattices. (b) Each added layer cycles around this stacking triangle in either the right-handed or the left-handed sense. Reversals of the sense of this rotation tend to increase the number of low-energy pseudospin doublets N_D . In graphite, Bernal (AB) stacking corresponds to a reversal at every step and orthorhombic (ABC) stacking corresponds to no reversals.

2.1. Stacking diagrams

When one graphene layer is placed on another, it is energetically favorable¹²⁾ for the atoms of either α or β sublattices to be displaced along the honeycomb edges, as illustrated in Fig. 1. This stacking rule implies the three distinct but equivalent projections (labeled A, B, and C) of the three-dimensional structure's honeycomb-lattice layers onto the \hat{x} - \hat{y} plane and 2^{N-2} distinct N -layer stack sequences. When a B layer is placed on an A layer, a C layer on a B layer, or an A layer on a C layer, the α sites of the upper layer are above the β sites of the lower layer and therefore linked by the nearest interlayer neighbor π -orbital hopping amplitude t_\perp . For the corresponding anticyclic stacking choices (A on B, B on C, or C on A), it is the β sites of the upper layer and the α sites of the lower layer that are linked. All distinct $N = 3$, $N = 4$, and $N = 5$ layer stacks are illustrated in Fig. 2, in which we have arbitrarily labeled the first two layers starting from the bottom as A and B.

2.2. Energy band structure

2.2.1. Preliminaries

Before analyzing energy spectrum of multilayer graphene, let us consider the Hamiltonian of a one-band tight-binding model for a chain of length N with near-

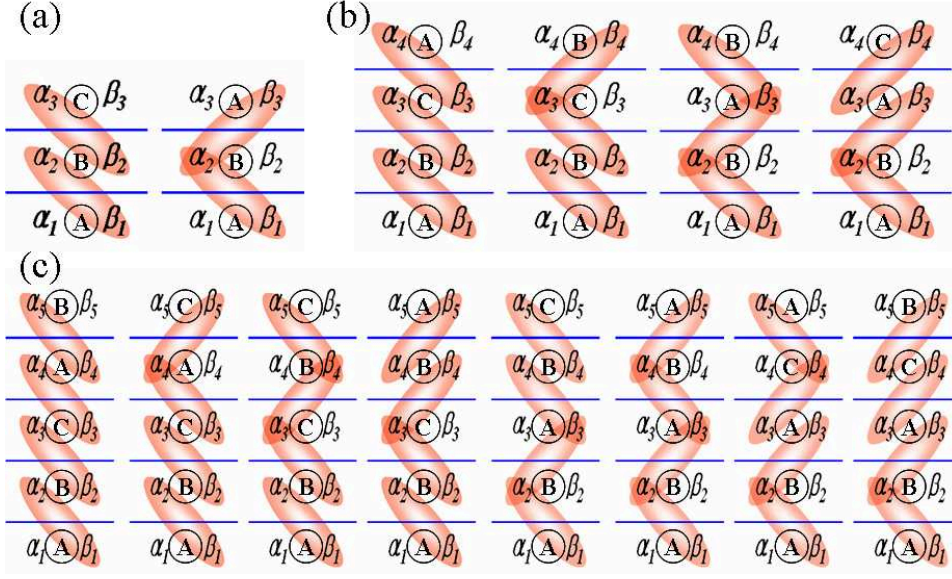


Fig. 2. (Color online) Stacking sequences and linkage diagrams for $N = 3, 4, 5$ layer stacks. The low-energy band and Landau level structures of a graphene stacks with nearest-neighbor hopping are readily read off these diagrams as explained in the text. Shaded ovals link α and β nearest interlayer neighbors.

neighbor hopping parameter t_{\perp} :

$$H = \begin{pmatrix} 0 & t_{\perp} & 0 & 0 & & \\ t_{\perp} & 0 & t_{\perp} & 0 & & \\ 0 & t_{\perp} & 0 & t_{\perp} & \cdots & \\ 0 & 0 & t_{\perp} & 0 & & \\ & & \cdots & & & \end{pmatrix}. \quad (2.2)$$

This Hamiltonian is important for analyzing the role of interlayer hopping as we explain below.

Let $\mathbf{a} = (a_1, \dots, a_N)$ be an eigenvector with an eigenvalue ε . Then the eigenvalue problem reduces to the following difference equation

$$\varepsilon a_n = t_{\perp}(a_{n-1} + a_{n+1}), \quad (2.3)$$

with the boundary condition $a_0 = a_{N+1} = 0$. Assuming $a_n \sim e^{in\theta}$, it can be shown that¹³⁾

$$\begin{aligned} \varepsilon_r &= 2t_{\perp} \cos \theta_r, \\ \mathbf{a}_r &= \sqrt{\frac{2}{N+1}} (\sin \theta_r, \sin 2\theta_r, \dots, \sin N\theta_r), \end{aligned} \quad (2.4)$$

where $r = 1, 2, \dots, N$ is the chain eigenvalue index and $\theta_r = r\pi/(N+1)$. Note that odd N chains have a zero-energy eigenstate with an eigenvector that has nonzero amplitudes, constant in magnitude and alternating in sign, on the sublattice of the chain ends.

2.2.2. AA stacking

Although AA stacking is not energetically favorable, it is still interesting to consider this arrangement for pedagogical purposes. In the case of AA stacking, the Hamiltonian at K is given by

$$H_{AA}(\mathbf{p}) = \begin{pmatrix} 0 & v\pi^\dagger & t_\perp & 0 & 0 & 0 \\ v\pi & 0 & 0 & t_\perp & 0 & 0 \\ t_\perp & 0 & 0 & v\pi^\dagger & t_\perp & 0 \\ 0 & t_\perp & v\pi & 0 & 0 & t_\perp & \cdots \\ 0 & 0 & t_\perp & 0 & 0 & v\pi^\dagger \\ 0 & 0 & 0 & t_\perp & v\pi & 0 \\ & & & \cdots & & \end{pmatrix}, \quad (2.5)$$

where $\pi = p_x + ip_y$.

As we now explain, the electronic structure of AA stacked N -layer graphene can be thought of as consisting of separate 1D chains for each wavevector in the 2D triangular lattice Brillouin zone of a single graphene layer. For an eigenvector $(a_1, b_1, \dots, a_N, b_N)$ with an eigenvalue ε and fixed 2D momentum, the difference equations in this case are

$$\begin{aligned} \varepsilon a_n &= t_\perp(a_{n-1} + a_{n+1}) + v\pi^\dagger b_n, \\ \varepsilon b_n &= t_\perp(b_{n-1} + b_{n+1}) + v\pi a_n, \end{aligned} \quad (2.6)$$

with the boundary condition $a_0 = a_{N+1} = b_0 = b_{N+1} = 0$.

Let $c_n = a_n + b_n e^{-i\phi}$ and $d_n = a_n - b_n e^{-i\phi}$ where $\phi = \tan^{-1}(p_y/p_x)$, then

$$\begin{aligned} (\varepsilon - v|\mathbf{p}|)c_n &= t_\perp(c_{n-1} + c_{n+1}), \\ (\varepsilon + v|\mathbf{p}|)d_n &= t_\perp(d_{n-1} + d_{n+1}), \end{aligned} \quad (2.7)$$

with the same boundary condition $c_0 = c_{N+1} = d_0 = d_{N+1} = 0$. Thus the energy spectrum is given by

$$\varepsilon_{r,\mathbf{p}}^\pm = \pm v|\mathbf{p}| + 2t_\perp \cos\left(\frac{r\pi}{N+1}\right), \quad (2.8)$$

where $r = 1, 2, \dots, N$. Note that for odd N , the $r = (N+1)/2$ mode provides two zero-energy states at $\mathbf{p} = 0$.

Figure 3 shows the band structure of AA stacked trilayer and tetralayer graphene near the K point. Because of the hybridization between α - α and β - β sublattices in each layer, zero-energy states occur at momenta that are remote from the K and K' points. In the following we turn our attention to stacks in which adjacent graphene layers have a relative rotation of 60 degrees. As we show, in this case the zero-energy states always occur precisely at the Brillouin-zone corners.

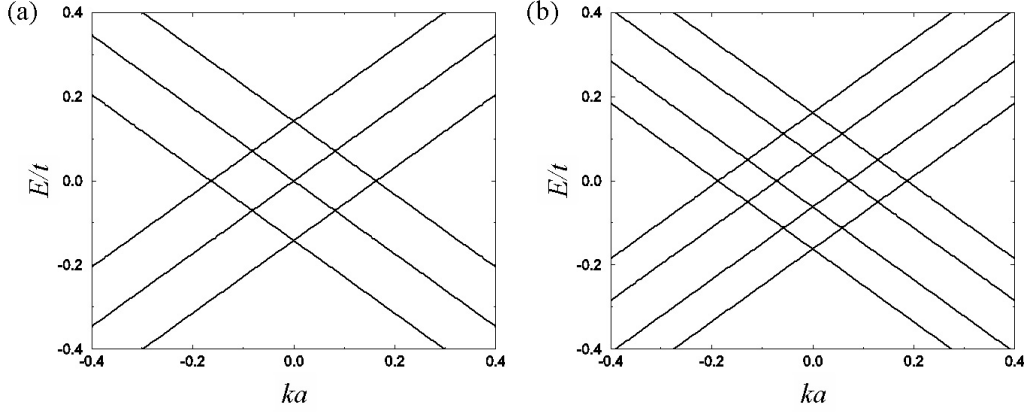


Fig. 3. Band structure near the K point for (a) trilayer and (b) tetralayer graphene with AA stacking for nearest intralayer neighbor hopping $t = 3$ eV and nearest interlayer neighbor hopping $t_{\perp} = 0.1t$.

2.2.3. AB stacking

In the case of AB stacking, the Hamiltonian at K has the following form,

$$H_{AB}(\mathbf{p}) = \begin{pmatrix} 0 & v\pi^{\dagger} & 0 & 0 & 0 & 0 & \dots \\ v\pi & 0 & t_{\perp} & 0 & 0 & 0 & \dots \\ 0 & t_{\perp} & 0 & v\pi^{\dagger} & 0 & t_{\perp} & \dots \\ 0 & 0 & v\pi & 0 & 0 & 0 & \dots \\ 0 & 0 & 0 & 0 & 0 & v\pi^{\dagger} & \dots \\ 0 & 0 & t_{\perp} & 0 & v\pi & 0 & \dots \\ \dots & \dots & \dots & \dots & \dots & \dots & \dots \end{pmatrix}. \quad (2.9)$$

We will see that the subtle difference in the Hamiltonian compared to the AA case changes the electronic structure in a qualitative way. To obtain the energy spectrum of AB stacked N -layer graphene, let us consider corresponding difference equations:¹⁴⁾

$$\begin{aligned} \varepsilon a_{2n-1} &= (v\pi^{\dagger})b_{2n-1}, \\ \varepsilon b_{2n-1} &= t_{\perp}(a_{2n-2} + a_{2n}) + (v\pi)a_{2n-1}, \\ \varepsilon a_{2n} &= t_{\perp}(b_{2n-1} + b_{2n+1}) + (v\pi^{\dagger})b_{2n}, \\ \varepsilon b_{2n} &= (v\pi)a_{2n}, \end{aligned} \quad (2.10)$$

with the boundary condition $a_0 = a_{N+1} = b_0 = b_{N+1} = 0$.

Let $c_{2n-1} = b_{2n-1}$ and $c_{2n} = a_{2n}$, then the difference equations reduce to

$$(\varepsilon - v^2|\mathbf{p}|^2/\varepsilon)c_n = t_{\perp}(c_{n-1} + c_{n+1}), \quad (2.11)$$

with the boundary condition $c_0 = c_{N+1} = 0$. Then the energy spectrum is given by

$$\varepsilon - v^2|\mathbf{p}|^2/\varepsilon = 2t_{\perp} \cos\left(\frac{r\pi}{N+1}\right), \quad (2.12)$$

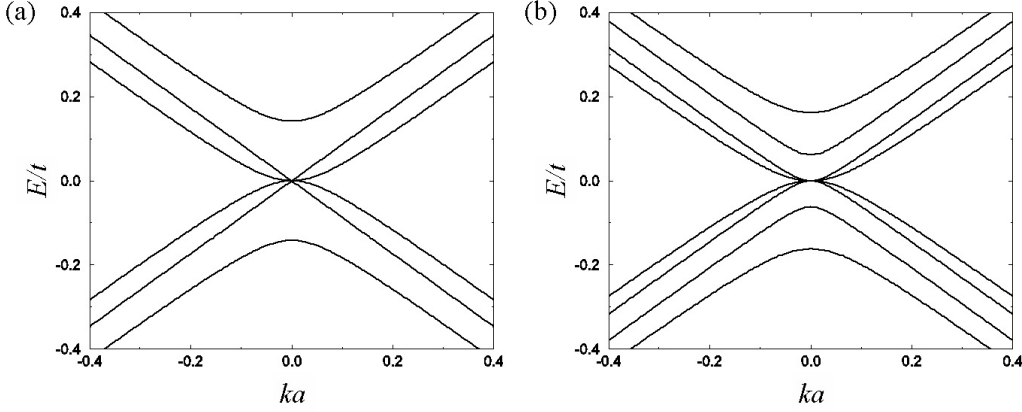


Fig. 4. Band structure near the K point for (a) trilayer and (b) tetralayer graphene with AB stacking for nearest intralayer neighbor hopping $t = 3$ eV and nearest interlayer neighbor hopping $t_{\perp} = 0.1t$.

where $r = 1, 2, \dots, N$. Thus

$$\varepsilon_{r,\mathbf{p}}^{\pm} = t_{\perp} \cos\left(\frac{r\pi}{N+1}\right) \pm \sqrt{v^2|\mathbf{p}|^2 + t_{\perp}^2 \cos^2\left(\frac{r\pi}{N+1}\right)}. \quad (2.13)$$

Note that relativistic energy spectrum for a particle with the momentum \mathbf{p} and mass m is given by

$$\varepsilon_{\mathbf{p}} = \sqrt{|\mathbf{p}|^2 c^2 + m^2 c^4}. \quad (2.14)$$

Thus we can identify $m_r v^2 = \left| t_{\perp} \cos\left(\frac{r\pi}{N+1}\right) \right|$ as the effective mass for mode r .

For a massive mode with mass m_r , the low-energy spectrum is given by

$$\varepsilon_{r,\mathbf{p}} \approx \begin{cases} +\frac{\mathbf{p}^2}{2m_r} & \text{if } t_{\perp} \cos\left(\frac{r\pi}{N+1}\right) < 0, \\ -\frac{\mathbf{p}^2}{2m_r} & \text{if } t_{\perp} \cos\left(\frac{r\pi}{N+1}\right) > 0. \end{cases} \quad (2.15)$$

For odd N , the mode with $r = (N+1)/2$ is massless and its energy is given by

$$\varepsilon_{\mathbf{p}}^{\pm} \approx \pm v|\mathbf{p}|. \quad (2.16)$$

For even N , all N modes are massive at low energies. Therefore, the low-energy spectrum with odd number of layers is a combination of one massless Dirac mode and $N-1$ massive Dirac modes, whereas the low-energy spectrum with even number of layers is composed of only massive Dirac modes.

Figure 4 shows the band structure of AB stacked trilayer and tetralayer graphene near the K point. As discussed earlier, the trilayer has one massless mode and two massive modes, while the tetralayer has all massive modes at low energies. Note that at $\mathbf{p} = 0$, each massless mode gives two zero energies while each massive mode gives one zero energy. Therefore, for odd N , there are $2 + (N-1) = N+1$ zero-energy states while for even N , there are N zero-energy states.

2.2.4. ABC stacking

In the case of ABC stacking, the Hamiltonian at K is given by

$$H_{\text{ABC}}(\mathbf{p}) = \begin{pmatrix} 0 & v\pi^\dagger & 0 & 0 & 0 & 0 & \cdots \\ v\pi & 0 & t_\perp & 0 & 0 & 0 & \\ 0 & t_\perp & 0 & v\pi^\dagger & 0 & 0 & \\ 0 & 0 & v\pi & 0 & t_\perp & 0 & \\ 0 & 0 & 0 & t_\perp & 0 & v\pi^\dagger & \\ 0 & 0 & 0 & 0 & v\pi & 0 & \\ \cdots & & & & & & \end{pmatrix}. \quad (2.17)$$

Unfortunately for ABC stacking, there do not exist low-order difference equations with a simple boundary condition. Instead we can easily derive a low-energy effective Hamiltonian. Surprisingly, it turns out that ABC stacked N -layer graphene is described by N -chiral 2D electron system. (More detailed discussion for the effective theory of arbitrarily stacked graphene will be presented in §3.)

It is important to recognize that in ABC stacking, there is vertical hopping between all the lower layer β sites and all the upper layer α sites. For $\pi = 0$ each α - β pair forms a symmetric-antisymmetric doublet with energies $\pm t_\perp$, leaving the bottom α_1 and top β_N sites as the only low-energy states. This behavior is readily understood from the stacking diagrams, in Fig. 2. It is possible to construct a 2×2 π -dependent low-energy effective Hamiltonian for the low-energy part of the spectrum using perturbation theory. The same procedure can then be extended to arbitrary stacking sequences.

The simplest example is bilayer graphene.¹⁵⁾ Low and high energy subspaces are identified by finding the spectrum at $\pi = 0$ and identifying all the zero-energy eigenstates. The intralayer tunneling term, which is proportional to π , couples low and high energy states. Using degenerate state perturbation theory, the effective Hamiltonian in the low energy space is given to leading (2nd) order in π by

$$H_2^{\text{eff}}(\mathbf{p}) = - \begin{pmatrix} 0 & \frac{(\pi^\dagger)^2}{2m} \\ \frac{(\pi)^2}{2m} & 0 \end{pmatrix} = -t_\perp \begin{pmatrix} 0 & (\nu^\dagger)^2 \\ (\nu)^2 & 0 \end{pmatrix}, \quad (2.18)$$

where we have used a (α_1, β_2) basis, $m = t_\perp/2v^2$ and $\nu = v\pi/t_\perp$. In the same way we find that the effective Hamiltonian of ABC stacked N -layer graphene is given by

$$H_N^{\text{eff}}(\mathbf{p}) = -t_\perp \begin{pmatrix} 0 & (\nu^\dagger)^N \\ (\nu)^N & 0 \end{pmatrix}, \quad (2.19)$$

using a (α_1, β_N) basis. The leading correction appears at order N in π because the unperturbed high-energy states are localized on a (β_i, α_{i+1}) pair and the perturbation is intralayer tunneling. Note that we have for mathematical convenience chosen a gauge in which the single-layer Hamiltonian is

$$H_1^{\text{eff}}(\mathbf{p}) = - \begin{pmatrix} 0 & v\pi^\dagger \\ v\pi & 0 \end{pmatrix}. \quad (2.20)$$

We can prove Eq. (2.19) by the mathematical induction method. Imagine that we add one more layer on top of N -layer graphene with ABC stacking. Then the combined Hamiltonian is given by

$$H_{N+1}^{eff}(\mathbf{p}) = -t_{\perp} \begin{pmatrix} 0 & (\nu^{\dagger})^N & 0 & 0 \\ (\nu)^N & 0 & -1 & 0 \\ 0 & -1 & 0 & \nu^{\dagger} \\ 0 & 0 & \nu & 0 \end{pmatrix}, \quad (2.21)$$

using a $(\alpha_1, \beta_N, \alpha_{N+1}, \beta_{N+1})$ basis.

Let P be a low-energy subspace spanned by (α_1, β_{N+1}) and Q be a high-energy subspace spanned by (α_{N+1}, β_N) . Note that the effective Hamiltonian can be derived using the degenerate state perturbation theory,¹⁶⁾

$$H_{eff} \approx H_{PP} - H_{PQ} \frac{1}{H_{QQ}} H_{QP}. \quad (2.22)$$

Here the projected Hamiltonian matrices to P and Q subspace are given by

$$H_{QQ}(\mathbf{p}) = t_{\perp} \begin{pmatrix} 0 & 1 \\ 1 & 0 \end{pmatrix}, \quad H_{PQ}(\mathbf{p}) = -t_{\perp} \begin{pmatrix} 0 & (\nu^{\dagger})^N \\ \nu & 0 \end{pmatrix}, \quad (2.23)$$

and $H_{PP}(\mathbf{p}) = 0$. Thus we can easily show that,

$$H_{N+1}^{eff}(\mathbf{p}) \approx -t_{\perp} \begin{pmatrix} 0 & (\nu^{\dagger})^{N+1} \\ (\nu)^{N+1} & 0 \end{pmatrix}, \quad (2.24)$$

which proves Eq. (2.19). The corresponding energy spectrum in Eq. (2.19) is given by

$$\varepsilon_{eff,\mathbf{p}}^{\pm} = \pm t_{\perp} \left(\frac{v|\mathbf{p}|}{t_{\perp}} \right)^N. \quad (2.25)$$

Figure 5 shows the band structure of ABC stacked trilayer and tetralayer graphene near the K point. Note that at $\mathbf{p} = 0$, there are only two zero energy states no matter how thick the stack is.

2.2.5. Arbitrary stacking

It is easy to generalize the previous discussion to construct the Hamiltonian for an arbitrarily stacked multilayer graphene system. Figure 6 shows the band structure of ABCB stacked tetralayer graphene and ABBC stacked tetralayer graphene near the K point. For the ABCB stacked tetralayer graphene, the low-energy spectrum looks like a superposition of a linear dispersion and a cubic one. For the ABBA stacked tetralayer graphene, zero energies appear not only at the Dirac point but also away from it. A more detailed low-energy spectrum analysis will be presented in §3.

2.3. Landau level spectrum

2.3.1. Preliminaries

In the presence of a magnetic field $\mathbf{B} = B\hat{z}$, a Hamiltonian is modified by $\mathbf{p} \rightarrow \mathbf{p} + \frac{e}{c}\mathbf{A}$, where \mathbf{A} is the vector potential with $\mathbf{B} = \nabla \times \mathbf{A}$. The quantum

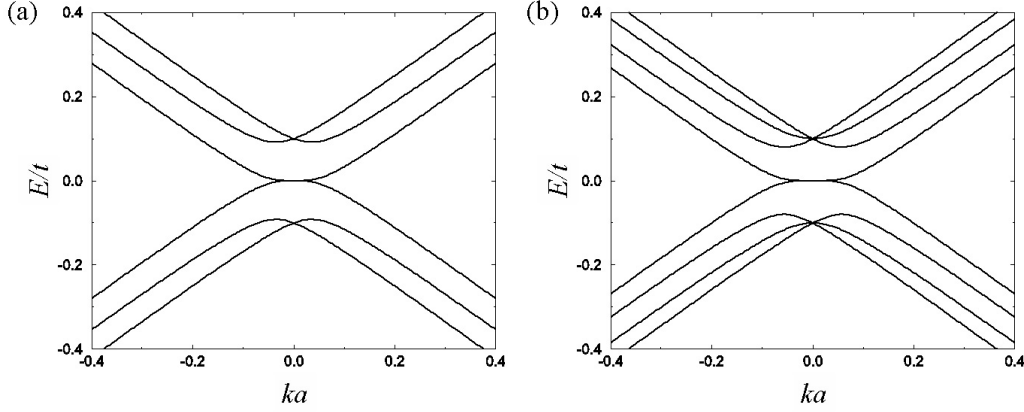


Fig. 5. Band structure near the K point for (a) trilayer and (b) tetralayer graphene with ABC stacking for nearest intralayer neighbor hopping $t = 3$ eV and nearest interlayer neighbor hopping $t_{\perp} = 0.1t$.

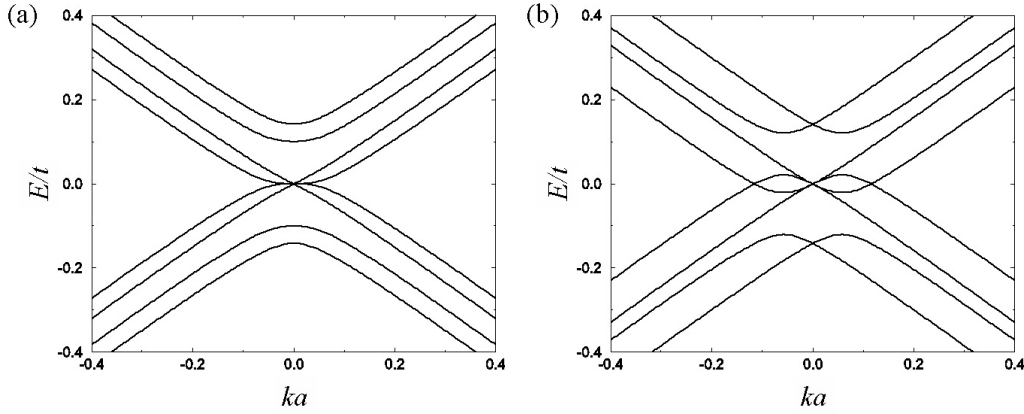


Fig. 6. Band structure near the K point for tetralayer graphene with (a) ABCB stacking and (b) ABBC stacking for nearest intralayer neighbor hopping $t = 3$ eV and nearest interlayer neighbor hopping $t_{\perp} = 0.1t$.

Hamiltonian is most easily diagonalized by introducing raising and lowering operators, $a = l\pi^{\dagger}/\sqrt{2}\hbar$ and $a^{\dagger} = l\pi/\sqrt{2}\hbar$ substitution, where $l = \sqrt{\hbar c/e|B|}$, and noting that $[a, a^{\dagger}] = 1$. We can then expand the wavefunction amplitude on each sublattice of each layer in terms of parabolic band Landau level states $|n\rangle$ which are eigenstates of the $a^{\dagger}a$. For many Hamiltonians, including those studied here, the Hamiltonian can be block diagonalized by fixing the parabolic band Landau-level offset between different sublattices and between different layers. This procedure is familiar from theories of Landau-level structure in other multiband $\mathbf{k} \cdot \mathbf{p}$ theories.

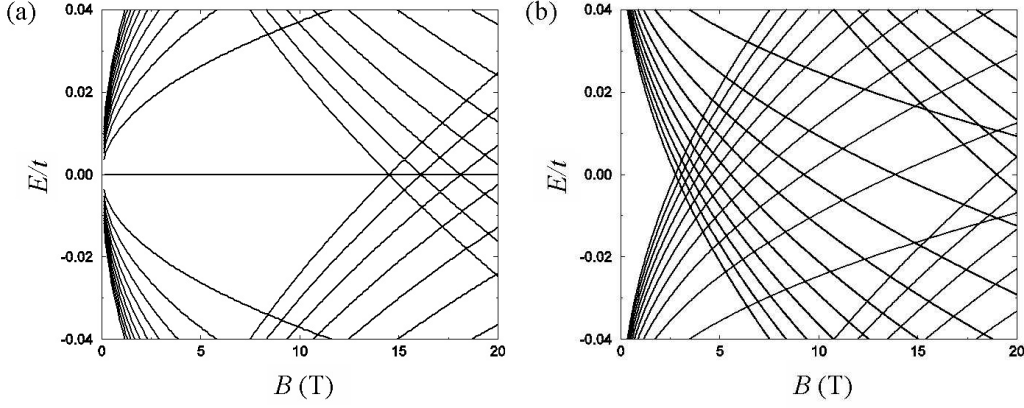


Fig. 7. Landau levels of (a) trilayer and (b) tetralayer graphene with AA stacking for nearest intralayer neighbor hopping $t = 3$ eV and nearest interlayer neighbor hopping $t_{\perp} = 0.1t$. Landau levels were shown up to $n = 10$.

2.3.2. AA stacking

In the case of AA stacking, let us choose the n -th Landau level basis at K as $(\alpha_{1,n-1}, \beta_{1,n}, \dots, \alpha_{N,n-1}, \beta_{N,n})$. Then Eq. (2.5) reduces to

$$H_{AA}(n) = \begin{pmatrix} 0 & \varepsilon_n & t_{\perp} & 0 & 0 & 0 \\ \varepsilon_n & 0 & 0 & t_{\perp} & 0 & 0 \\ t_{\perp} & 0 & 0 & \varepsilon_n & t_{\perp} & 0 \\ 0 & t_{\perp} & \varepsilon_n & 0 & 0 & t_{\perp} & \cdots \\ 0 & 0 & t_{\perp} & 0 & 0 & \varepsilon_n & \\ 0 & 0 & 0 & t_{\perp} & \varepsilon_n & 0 & \end{pmatrix}, \quad (2.26)$$

where $\varepsilon_n = \sqrt{2n}\hbar v/l$. Note that 2D Landau level states with a negative index do not exist so the corresponding basis states and matrix elements are understood as being absent in the matrix block. Thus $H_{AA}(n=0)$ is a $N \times N$ matrix, while $H_{AA}(n>0)$ is a $2N \times 2N$ matrix.

By diagonalizing Eq. (2.26) using the difference equation method, we can obtain the exact Landau level spectrum. For $n > 0$, Landau levels are given by

$$\varepsilon_{r,n}^{\pm} = \pm\varepsilon_n + 2t_{\perp} \cos\left(\frac{r\pi}{N+1}\right), \quad (2.27)$$

where $r = 1, 2, \dots, N$. Note that for $n = 0$, Landau levels are given by $\varepsilon_{r,0} = 2t_{\perp} \cos\left(\frac{r\pi}{N+1}\right)$. Thus for odd N , there exists one (B -independent) zero-energy Landau level at $r = (N+1)/2$.

Figure 7 shows the Landau levels of AA stacked trilayer and tetralayer graphene as a function of magnetic fields. For the trilayer, there is one zero-energy Landau level, while for the tetralayer, there is no zero-energy Landau level. Note that there are Landau levels crossing the zero-energy line in AA stacking.

2.3.3. AB stacking

In the case of AB stacking, a proper choice of the n -th Landau level basis at K is $(\alpha_{1,n-1}, \beta_{1,n}, \alpha_{2,n}, \beta_{2,n+1}, \alpha_{3,n-1}, \beta_{3,n}, \alpha_{4,n}, \beta_{4,n+1}, \dots)$ such that all the interlayer hopping terms are contained in the n -th Landau level Hamiltonian. Then Eq. (2.9) reduces to

$$H_{AB}(n) = \begin{pmatrix} 0 & \varepsilon_n & 0 & 0 & 0 & 0 \\ \varepsilon_n & 0 & t_{\perp} & 0 & 0 & 0 \\ 0 & t_{\perp} & 0 & \varepsilon_{n+1} & 0 & t_{\perp} \\ 0 & 0 & \varepsilon_{n+1} & 0 & 0 & 0 \\ 0 & 0 & 0 & 0 & 0 & \varepsilon_n \\ 0 & 0 & t_{\perp} & 0 & \varepsilon_n & 0 \\ & & & \dots & & \end{pmatrix}, \quad (2.28)$$

where $\varepsilon_n = \sqrt{2n}\hbar v/l$. As discussed earlier, special care should be given for states with a negative index.

For the Hamiltonian in Eq. (2.28), there do not exist corresponding difference equations with a proper boundary condition, thus cannot be diagonalized analytically. From Eq. (2.15), however, we can find the low-energy Landau levels for massive mode with mass m_r as

$$\varepsilon_{r,n} \approx \begin{cases} +\hbar\omega_r\sqrt{n(n+1)} & \text{if } t_{\perp} \cos\left(\frac{r\pi}{N+1}\right) < 0, \\ -\hbar\omega_r\sqrt{n(n+1)} & \text{if } t_{\perp} \cos\left(\frac{r\pi}{N+1}\right) > 0, \end{cases} \quad (2.29)$$

where $\omega_r = e|B|/m_rc$ and $r = 1, 2, \dots, N$, which is proportional to B . These equations apply at small B , just as the $B = 0$ limiting low-energy dispersions applied at small momentum π . For the massless mode, from Eq. (2.16) Landau levels are given by

$$\varepsilon_n^{\pm} = \pm\varepsilon_n, \quad (2.30)$$

which is proportional to $B^{1/2}$.

Figure 8 shows the Landau levels of AB stacked trilayer and tetralayer graphene as a function of magnetic fields. Note that the linear B dependence expected for massive modes applies over a more limited field range when the mass is small. For the trilayer, Landau levels are composed of massless Dirac spectra ($\propto B^{1/2}$) and massive Dirac spectra ($\propto B$), while for the tetralayer, Landau levels are all massive Dirac spectra. This is consistent with the band structure analysis shown in Fig. 4.

Note that the massive modes in Eq. (2.29) have two zero-energy Landau levels for $n = -1$ and 0 , whereas the massless mode in Eq. (2.30) has one for $n = 0$. There are therefore N zero-energy Landau levels in both even and odd N AB stacks. This property can also be understood directly from the Hamiltonian in Eq. (2.28), by eliminating negative n basis states and rearranging rows to block diagonalize the matrix.

2.3.4. ABC stacking

In the case of ABC stacking, a proper choice of the n -th Landau level basis at K is $(\alpha_{1,n-1}, \beta_{1,n}, \alpha_{2,n}, \beta_{2,n+1}, \alpha_{3,n+1}, \beta_{3,n+2}, \dots)$ such that all the interlayer hopping terms

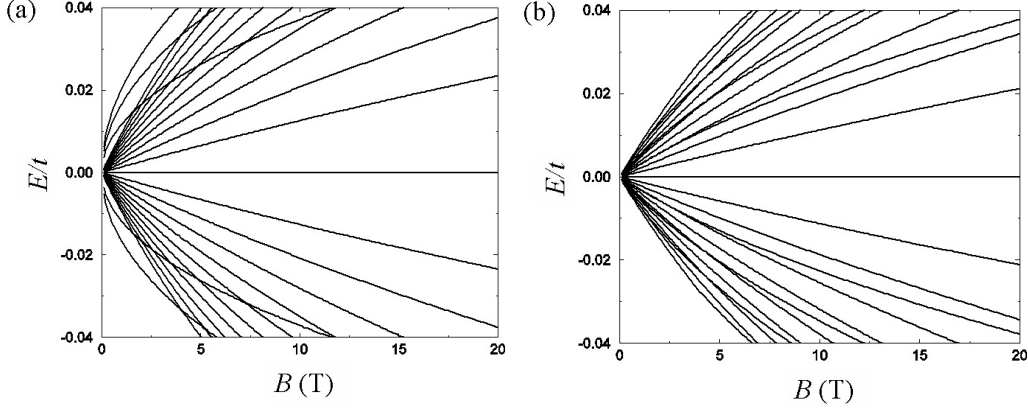


Fig. 8. Landau levels of (a) trilayer and (b) tetralayer graphene with AB stacking for nearest intralayer neighbor hopping $t = 3$ eV and nearest interlayer neighbor hopping $t_{\perp} = 0.1t$. Landau levels up to $n = 10$ are shown.

are contained in the n -th Landau level Hamiltonian. Then Eq. (2·17) reduces to

$$H_{\text{ABC}}(n) = \begin{pmatrix} 0 & \varepsilon_n & 0 & 0 & 0 & 0 \\ \varepsilon_n & 0 & t_{\perp} & 0 & 0 & 0 \\ 0 & t_{\perp} & 0 & \varepsilon_{n+1} & 0 & 0 \\ 0 & 0 & \varepsilon_{n+1} & 0 & t_{\perp} & 0 \\ 0 & 0 & 0 & t_{\perp} & 0 & \varepsilon_{n+2} \\ 0 & 0 & 0 & 0 & \varepsilon_{n+2} & 0 \\ \vdots & \vdots & \vdots & \vdots & \vdots & \vdots \end{pmatrix}, \quad (2\cdot31)$$

where $\varepsilon_n = \sqrt{2n}\hbar v/l$.

The low-energy spectrum can be obtained from the effective Hamiltonian in Eq. (2·19). For $n > 0$, Landau levels are given by

$$\varepsilon_n^{\pm} = \pm \hbar \omega_N \sqrt{n(n+1) \cdots (n+N-1)}, \quad (2\cdot32)$$

where $\hbar \omega_N = t_{\perp}(\sqrt{2}\hbar v/t_{\perp}l)^N \propto B^{N/2}$, while for $n = -N+1, -N+2, \dots, 0$ they are zero. Note that there are N zero-energy Landau levels for ABC stacked N -layer graphene.

Figure 9 shows the Landau levels of ABC stacked trilayer and tetralayer graphene as a function of magnetic fields. For the trilayer, Landau levels are proportional to $B^{3/2}$, while for the tetralayer, Landau levels are proportional to B^2 .

2.3.5. Arbitrary stacking

It is straightforward to generalize the previous discussion to construct the Hamiltonian in Landau level basis for an arbitrarily stacked multilayer graphene system. As discussed earlier, special care should be given for states with a negative index. Figure 10 shows Landau levels of ABCB stacked tetralayer graphene and ABBC stacked tetralayer graphene. For the ABCB stacked tetralayer graphene, the Landau levels look like a superposition of $B^{1/2}$ and $B^{3/2}$ levels, which is consistent with

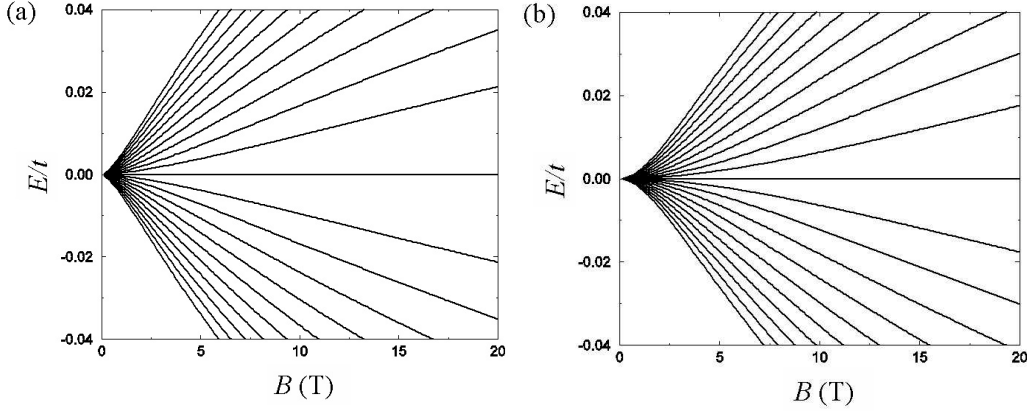


Fig. 9. Landau levels of (a) trilayer and (b) tetralayer graphene with ABC stacking for nearest intralayer neighbor hopping $t = 3$ eV and nearest interlayer neighbor hopping $t_{\perp} = 0.1t$. Landau levels up to $n = 10$ are shown.

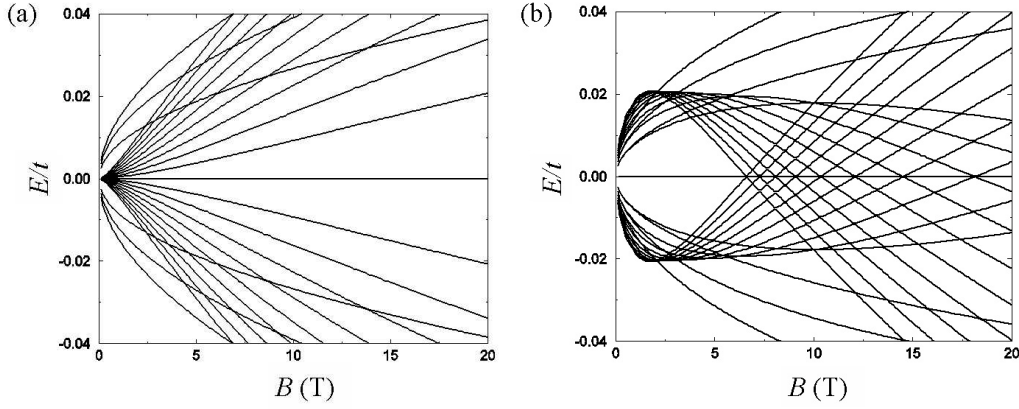


Fig. 10. Landau levels of tetralayer graphene with (a) ABCB stacking and (b) ABBC stacking for nearest intralayer neighbor hopping $t = 3$ eV and nearest interlayer neighbor hopping $t_{\perp} = 0.1t$. Landau levels up to $n = 10$ are shown.

Fig. 6(a). For the ABBA stacked tetralayer graphene, there are Landau levels crossing the zero-energy line, which is consistent with Fig. 6(b). Detailed low-energy Landau-level spectrum analysis will be presented in §3.

2.4. Quantum Hall conductivity

Applying the Kubo formula to a disorder-free systems we find that the conductivity tensor with an external magnetic field along z is given by

$$\sigma_{ij}(\omega) = -\frac{e^2}{2\pi\hbar l_B^2} \sum_n f_n \Omega_{ij}^n(\omega), \quad (2.33)$$

where f_n is Fermi factor of n -th energy state, $i, j = x, y$ and

$$\Omega_{ij}^n(\omega) = i \sum_{m \neq n} \left[\frac{\langle n | \hbar v_i | m \rangle \langle m | \hbar v_j | n \rangle}{(\varepsilon_n - \varepsilon_m)(\varepsilon_n - \varepsilon_m + \hbar\omega + i\eta)} - \frac{\langle m | \hbar v_i | n \rangle \langle n | \hbar v_j | m \rangle}{(\varepsilon_n - \varepsilon_m)(\varepsilon_n - \varepsilon_m - \hbar\omega - i\eta)} \right]. \quad (2.34)$$

Here v_i is a velocity operator obtained by taking a derivative of the Hamiltonian $H(\mathbf{p})$ with respect to p_i . Note that in case of multilayer graphene, the velocity operator is constant, i.e. it does not depend on the Landau level index.

The appropriate quantized Hall conductivity is obtained by evaluating $\sigma_H = \sigma_{xy}(0)$. Detailed analysis of the quantum Hall conductivity will be presented in §3.

§3. Chiral decomposition of energy spectrum

In this section^{*)} we demonstrate an unanticipated low-energy property of graphene multilayers, which follows from an interplay between interlayer tunneling and the chiral properties of low-energy quasiparticles in an isolated graphene sheet. Our conclusions apply in the strongest form to models with only nearest-neighbor interlayer tunneling, but are valid over a broad field range as we explain below. We find that the low-energy band structure of any graphene multilayer consists of a set of independent pseudospin doublets. Within each doublet, the bands are described by a pseudospin Hamiltonian of the form

$$H_J(\mathbf{k}) \propto k^J [\cos(J\phi_{\mathbf{k}}) \tau^x \pm \sin(J\phi_{\mathbf{k}}) \tau^y], \quad (3.1)$$

where τ^α is a Pauli matrix acting on the doublet pseudospin, \mathbf{k} is an envelope function momentum measured from either the K or K' corner of the honeycomb lattice's Brillouin-zone,^{1),2)} $k = |\mathbf{k}|$, and $\phi_{\mathbf{k}}$ is the orientation of \mathbf{k} . The \pm sign in Eq. (3.1) assumes the opposite signs in graphene's K and K' valleys. Following the earlier work on graphene bilayers,¹⁵⁾ we refer to J as the chirality index of a doublet. In the presence of a perpendicular magnetic field B , $H_J(\mathbf{k})$ yields J Landau levels at $E = 0$ and $E \neq 0$ levels with $|E| \propto B^{J/2}$. Taking the twofold spin and valley degeneracies into account, the number of independent zero-energy band eigenstates at the Dirac point ($\mathbf{k} = 0$) is therefore $8N_D$, where N_D is the number of pseudospin doublets. We find that, although N_D depends on the details of the stacking sequence,

$$\sum_{i=1}^{N_D} J_i = N \quad (3.2)$$

in an N -layer stack. It follows from Eq. (3.2) that the Hall conductivity of an N -layer stack has strong integer quantum Hall effects with plateau conductivities,

$$\sigma_{xy} = \pm \frac{4e^2}{h} \left(\frac{N}{2} + n \right), \quad (3.3)$$

where n is a non-negative integer.

^{*)} The content of this section provides a more complete explanation of the arguments presented earlier in Ref. 10).

3.1. Partitioning rules

The low-energy band and the Landau level structure can be read off the stacking diagrams illustrated in Fig. 2 by partitioning a stack using the following rules, which are justified in the following section.

(i) Identify the longest nonoverlapping segments within which there are no reversals of stacking sense. When there is ambiguity in the selection of nonoverlapping segments, choose the partitioning which incorporates the largest number of layers. Each segment (including for interior segments the end layers at which reversals take place) defines a J -layer partition of the stack and may be associated with a chirality J doublet.

(ii) Iteratively partition the remaining segments of the stack into smaller J elements, excluding layers contained within previously identified partitions, until all layers are exhausted.

The chirality decompositions which follow from these rules are summarized in Table I. Note that this procedure can result in $J = 1$ doublets associated with separated single layers which remain at the last step in the partitioning process.

In applying these rules, the simplest case is cyclic ABC stacking for which there are no stacking sense reversals and therefore a single $J = N$ partition. In the opposite limit, AB stacking, the stacking sense is reversed in every layer and the rules imply $N/2$ partitions with $J = 2$ for even N , and when N is odd a remaining $J = 1$ partition. Between these two limits, a rich variety of qualitatively distinct low-energy behaviors occur. For example, in the ABCB stacked tetralayer, ABC is identified as a $J = 3$ doublet and the remaining B layer gives a $J = 1$ doublet. The low-energy band structure and the Landau level structure of this stack, as illustrated in Figs. 6(a) and 10(a), have two sets of low-energy bands with $|E| \propto k, k^3$, Landau levels with $|E| \propto B^{1/2}, B^{3/2}$, and four zero-energy Landau levels per spin and valley. All these properties are predicted by the partitioning rules. We have explicitly checked that the rules correctly reproduce the low-energy electronic structure for all stacking sequences up to $N = 7$. Because each layer is a member of one and only one partition, the partitioning rules imply the chirality sum rule in Eq. (3·2).

3.2. Degenerate state perturbation theory

We start from the well-known $J = 1$ massless Dirac equation^{1),2)} $\mathbf{k} \cdot \mathbf{p}$ model for isolated sheets,

$$H_{MD}(\mathbf{p}) = - \begin{pmatrix} 0 & v\pi^\dagger \\ v\pi & 0 \end{pmatrix}, \quad (3·4)$$

where $\pi = p_x + ip_y$ and v is the quasiparticle velocity. In the presence of an external magnetic field, π and π^\dagger are proportional to the Landau level raising and lowering operators, so that Eq. (3·4) implies the presence of one macroscopically degenerate Landau level at the Dirac point for each spin and valley, and therefore, to the $N = 1$ quantum Hall effect^{8),9)} of Eq. (3·3). An N -layer stack has a two-dimensional band structure with $2N$ atoms per unit cell. The Hamiltonian can be written as

$$H = H_\perp + H_\parallel, \quad (3·5)$$

Table I. Chirality decomposition for $N = 3, 4, 5, 6$ layer stacks.

stacking	chirality	stacking	chirality
ABC	3	ABCABC	6
ABA	2+1	ABCABA	5+1
		ABCACA	4+2
ABCA	4	ABCACB	4+2
ABCB	3+1	ABCBCA	3+3
ABAB	2+2	ABCBCB	3+2+1
ABAC	1+3	ABCBAB	3+2+1
		ABCBAC	3+3
ABCAB	5	ABABCA	2+4
ABCAC	4+1	ABABCB	2+3+1
ABCBC	3+2	ABABAB	2+2+2
ABCBA	3+2	ABABAC	2+1+3
ABABC	2+3	ABACAB	2+1+3
ABABA	2+2+1	ABACAC	1+3+2
ABACA	1+3+1	ABACBC	1+4+1
ABACB	1+4	ABACBA	1+5

where H_{\perp} accounts for interlayer tunneling and H_{\parallel} for intralayer tunneling. H_{\parallel} is the direct product of massless Dirac model Hamiltonians H_{MD} for the sublattice pseudospin degrees of freedom of each layer. We construct a low-energy Hamiltonian by first identifying the zero-energy eigenstates of H_{\perp} and then treating H_{\parallel} as a perturbation.

Referring to Fig. 2, we see that H_{\perp} is the direct product of a set of finite-length 1D tight-binding chains, as shown in Eq. (2.4), and a null matrix with dimension equal to the number of isolated sites. The set of zero-energy eigenstates of H_{\perp} consists of the states localized on isolated sites and the single zero-energy eigenstates of each odd-length chain.

The low-energy effective Hamiltonian is evaluated by applying leading order degenerate state perturbation theory to the zero-energy subspace. The matrix element of the effective Hamiltonian between degenerate zero-energy states r and r' is given by¹⁶⁾

$$\langle \Psi_r | H | \Psi_{r'} \rangle = \langle \Psi_r | H_{\parallel} \left[\hat{Q} (-H_{\perp}^{-1}) \hat{Q} H_{\parallel} \right]^{n-1} | \Psi_{r'} \rangle, \quad (3.6)$$

where n is the smallest positive integer for which the matrix element is nonzero, and $\hat{Q} = 1 - \hat{P}$, \hat{P} is a projection operator onto the zero-energy subspace. To understand the structure of this Hamiltonian, it is helpful to start with some simple examples.

3.2.1. ABC stacking

For ABC stacked N -layer graphene, the zero-energy states are the two isolated site states in bottom and top layers, α_1 and β_N . $N - 1$ sets of two-site chains form high-energy states. Because H_{\parallel} is diagonal in layer index and H_{\perp} (and hence H_{\perp}^{-1}) can change the layer index by one unit, the lowest order at which α_1 and β_N are coupled is $n = N$.

According to Eq. (2.4), the wavefunction of each two-site chain is given by

$$|\Phi_{\sigma_r}\rangle = \frac{1}{\sqrt{2}}(|\beta_r\rangle + \sigma_r |\alpha_{r+1}\rangle), \quad (3.7)$$

with the energy $\epsilon_r = t_\perp \sigma_r$, where $\sigma_r = \pm 1$ and $r = 1, 2, \dots, N-1$. From Eq. (3.6),

$$\begin{aligned} \langle \alpha_1 | H | \beta_N \rangle &= \langle \alpha_1 | H_\parallel \left[\hat{Q}(-H_\perp^{-1}) \hat{Q} H_\parallel \right]^{N-1} | \beta_N \rangle \\ &= \sum_{\{\sigma_r\}} \frac{\langle \alpha_1 | H_\parallel | \Phi_{\sigma_1} \rangle \cdots \langle \Phi_{\sigma_{N-1}} | H_\parallel | \beta_N \rangle}{(-\epsilon_1) \cdots (-\epsilon_{N-1})} \\ &= -t_\perp \sum_{\{\sigma_r\}} \frac{(-\sigma_1/2) \cdots (-\sigma_{N-1}/2)}{(-\sigma_1) \cdots (-\sigma_{N-1})} (\nu^\dagger)^N \\ &= -t_\perp (\nu^\dagger)^N \sum_{\sigma_1, \dots, \sigma_{N-1}} \frac{1}{2^{N-1}} \\ &= -t_\perp (\nu^\dagger)^N, \end{aligned} \quad (3.8)$$

where $\nu = v\pi/t_\perp$. Here $\langle \alpha_1 | V | \Phi_{\sigma_1} \rangle = -(1/\sqrt{2})t_\perp \nu^\dagger$, $\langle \Phi_{\sigma_{N-1}} | V | \beta_N \rangle = -(\sigma_{N-1}/\sqrt{2})t_\perp \nu^\dagger$ and $\langle \Phi_{\sigma_r} | V | \Phi_{\sigma_{r+1}} \rangle = -(\sigma_r/2)t_\perp \nu^\dagger$ were used. Thus, the effective Hamiltonian of N -layer graphene with ABC stacking has a single $J = N$ doublet given by

$$H_N^{eff} = -t_\perp \begin{pmatrix} 0 & (\nu^\dagger)^N \\ (\nu)^N & 0 \end{pmatrix}. \quad (3.9)$$

3.2.2. AB stacking

For AB stacked N -layer graphene, the high-energy Hilbert space consists of a single N -site 1D chain, excluding its zero-energy eigenstate when N is odd. There is an isolated site in each layer which is connected to both its neighbors at order $n = 2$ forming an isolated site chain. When N is even, this chain is diagonalized by $N/2$, $J = 2$ doublets formed between α -sublattice and β -sublattice chain states.^{(14), (17), (18), (19)} When N is odd, the zero-energy chain state is mapped to an equal-magnitude oscillating-sign linear combination of isolated site states by intralayer tunneling at order $n = 1$, yielding a $J = 1$ doublet. The $(N-1)/2$, $J = 2$ doublets are then formed between α -sublattice and β -sublattice isolated site chain states in the orthogonal portion of the isolated state subspace.

Let us consider the low-energy spectrum of AB stacking in more detail. From Eq. (2.4) energy spectra and wavefunctions of the single N -site chain are given by

$$\begin{aligned} \epsilon_r &= 2t_\perp \cos \theta_r, \\ |\Phi_r\rangle &= \sqrt{\frac{2}{N+1}} (\sin \theta_r |\beta_1\rangle + \sin 2\theta_r |\alpha_2\rangle + \sin 3\theta_r |\beta_3\rangle + \sin 4\theta_r |\alpha_4\rangle \cdots), \end{aligned} \quad (3.10)$$

where $\theta_r = \frac{r\pi}{N+1}$ and $r = 1, 2, \dots, N$.

First, let us consider the case with even N . Then the low-energy states come

from the isolated sites or equivalently their superpositions. Let us define

$$|\Psi_r\rangle = \sqrt{\frac{2}{N+1}} (\sin \theta_r e^{-i\phi} |\alpha_1\rangle + \sin 2\theta_r e^{i\phi} |\beta_2\rangle + \sin 3\theta_r e^{-i\phi} |\alpha_3\rangle + \sin 4\theta_r e^{i\phi} |\beta_4\rangle \cdots) \quad (3.11)$$

such that

$$\langle \Psi_r | V | \Phi_s \rangle = -\delta_{r,s} |\nu|, \quad (3.12)$$

where $e^{i\phi} = \nu/|\nu|$. Then the matrix elements between the low-energy states are given by the second order perturbation theory:

$$\langle \Psi_r | H | \Psi_{r'} \rangle = \sum_{s=1}^N \frac{\langle \Psi_r | V | \Phi_s \rangle \langle \Phi_s | V | \Psi_{r'} \rangle}{(-\varepsilon_s)} = -\delta_{r,r'} (t_\perp^2 / \varepsilon_r) |\nu|^2. \quad (3.13)$$

Note that $\varepsilon_r = -\varepsilon_{N+1-r}$ and these two modes form a 2-chiral system with energies $\pm|\varepsilon_r|$. The chirality can be manifested clearly if we define

$$\begin{aligned} |\tilde{\alpha}_r\rangle &= \frac{e^{i\phi}}{\sqrt{2}} (|\Psi_r\rangle + |\Psi_{N+1-r}\rangle), \\ |\tilde{\beta}_r\rangle &= \frac{e^{-i\phi}}{\sqrt{2}} (|\Psi_r\rangle - |\Psi_{N+1-r}\rangle). \end{aligned} \quad (3.14)$$

Then the Hamiltonian of the 2-chiral system for $r = 1, 2, \dots, N/2$ is given by

$$H_r = -\frac{t_\perp^2}{\varepsilon_r} \begin{pmatrix} 0 & (\nu^\dagger)^2 \\ (\nu)^2 & 0 \end{pmatrix} = -\begin{pmatrix} 0 & \frac{(\pi^\dagger)^2}{2m_r} \\ \frac{(\pi)^2}{2m_r} & 0 \end{pmatrix} \quad (3.15)$$

in a $(\tilde{\alpha}_r, \tilde{\beta}_r)$ basis with $m_r v^2 = t_\perp \cos\left(\frac{r\pi}{N+1}\right)$. Thus the system is described by a combination of massive Dirac modes with different masses.

For odd N , there is a zero-energy state in the N -site chain at $r = (N+1)/2$ in Eq. (3.10). Thus in addition to the massive modes, there exists one massless Dirac mode,

$$\langle \Psi_{\frac{N+1}{2}} | V | \Phi_{\frac{N+1}{2}} \rangle = -|\nu|. \quad (3.16)$$

Thus the system is described by one massless Dirac mode and a combination of massive Dirac modes with different masses.

3.2.3. ABC+B type stacking

A more complex and more typical example is realized by placing a single reversed layer on top of ABC stacked N -layer graphene with $N > 2$. Note that the last chain has three sites, thus it has a zero-energy state β_{N+1}^- defined by

$$|\beta_{N+1}^- \rangle = \frac{1}{\sqrt{2}} (|\beta_{N+1}\rangle - |\beta_{N-1}\rangle), \quad (3.17)$$

and two high-energy states with energies $\sqrt{2}\sigma_{N-1}t_\perp$ defined by

$$|\Phi_{\sigma_{N-1}}\rangle = \frac{1}{2} |\beta_{N-1}\rangle + \frac{\sigma_{N-1}}{\sqrt{2}} |\alpha_N\rangle + \frac{1}{2} |\beta_{N+1}\rangle, \quad (3.18)$$

where $\sigma_{N-1} = \pm 1$. Then the first-order perturbation theory gives

$$\langle \alpha_{N+1} | H | \beta_{N+1}^- \rangle = -\frac{t_\perp}{\sqrt{2}} \nu^\dagger, \quad (3.19)$$

suggesting the existence of the massless Dirac mode with a *reduced* velocity.

Similarly as Eq. (3.8), we obtain

$$H_{N+1}^{eff} = -t_\perp \begin{pmatrix} 0 & \frac{\nu^\dagger}{\sqrt{2}} & 0 & \frac{(\nu^\dagger)^2}{2} \\ \frac{\nu}{\sqrt{2}} & 0 & -\frac{(\nu)^{N-1}}{\sqrt{2}} & 0 \\ 0 & -\frac{(\nu^\dagger)^{N-1}}{\sqrt{2}} & 0 & \frac{(\nu^\dagger)^N}{2} \\ \frac{\nu^2}{2} & 0 & \frac{(\nu)^N}{2} & 0 \end{pmatrix}, \quad (3.20)$$

using a $(\alpha_{N+1}, \beta_{N+1}^-, \alpha_1, \beta_N)$ basis. The first 2×2 block in Eq. (3.20) gives a $J = 1$ doublet with a reduced velocity. Note that the matrix in Eq. (3.20) is not block diagonal thus we cannot simply say that the second 2×2 matrix block is a N -chiral system. The $J = N$ doublet in this instance includes both the (α_1, β_N) subspace contribution and an equal contribution due to perturbative coupling to the $(\alpha_{N+1}, \beta_{N+1}^-)$ subspace. Using a similar perturbation theory shown in Eq. (2.22), we can obtain higher order correction by integrating out the massless Dirac mode which forms a higher energy state. Then the final Hamiltonian is reduced to

$$H_{N+1}^{eff} \approx H_1 \otimes H_N, \quad (3.21)$$

where

$$H_1 = -t_\perp \begin{pmatrix} 0 & \nu^\dagger/\sqrt{2} \\ \nu/\sqrt{2} & 0 \end{pmatrix}, \quad H_N = -t_\perp \begin{pmatrix} 0 & (\nu^\dagger)^N \\ (\nu)^N & 0 \end{pmatrix}. \quad (3.22)$$

This means that the combined system can be described by a combination of one 1-chiral system with reduced velocity and one N -chiral system. Note that stacking a layer with an opposite handedness partitions a system into systems with different chiralities.

3.2.4. Arbitrary stacking

The relationship between the electronic structure of a general stack and the partitioning procedure explained above can be understood as follows.

(i) First, note that a partition with chirality J has isolated sites in its terminal layers that are coupled at order J in perturbation theory. In the case of $J = 1$ partition, the chain opposite to the single isolated site always has an odd length and provides the zero-energy partner; isolated site to chain coupling therefore always occurs at first order.

(ii) Next, consider the perturbation theory, truncating at successively higher orders. When truncated at first order, the $J = 1$ partitions are isolated by higher J blocks within which the Hamiltonian vanishes. Each $J = 1$ partition therefore yields a separate massless Dirac equation with velocities^{*)} that can be smaller than

^{*)} The velocity of the $J = 1$ doublets is determined by the strength of the coupling between

the graphene sheet Dirac velocity. When the perturbation theory is truncated at second order, the Hamiltonian becomes nonzero within the $J = 2$ partitions. The eigenenergies within the $J = 1$ partitions are parametrically larger, and the Hamiltonian within the $J > 2$ partitions is still zero. To leading order therefore, the $J = 2$ partitions are separated, and their isolated states are coupled at the second order in perturbation theory so that each provides a $J = 2$ doublet such as that of an isolated bilayer. If two or more $J = 2$ partitions are adjacent, then their Hamiltonians do not separate. In this case, there is a chain of second order couplings between isolated states, such as those of an even-length AB stack, but the end result is still $J = 2$ doublet for each $J = 2$ partition.

(iii) The identification between partitions and chiral doublets can be established by continuing this consideration up to the highest values of J which occur for a particular stack.

(iv) Then, the effective Hamiltonian of any N -layer graphene is as follows:

$$H_N^{eff} \approx H_{J_1} \otimes H_{J_2} \otimes \cdots \otimes H_{J_{N_D}}, \quad (3.23)$$

with the sum rule in Eq. (3.2). Note that N_D is half the sum of the number of isolated sites and the number of odd-length chains.

3.3. Discussion

3.3.1. Effects of remote hopping

The minimal model we have used to derive these results is approximately valid in the broad intermediate magnetic field B range between ~ 10 and ~ 100 T, over which the intralayer hopping energy in field ($\sim \hbar v / \ell$ where $\ell = \sqrt{\hbar c / e |B|} \sim 25 \text{ nm} / [B(\text{T})]^{1/2}$ is the magnetic length) is larger than the distant neighbor interlayer hopping amplitudes that we have neglected ($\gamma_2 \sim -20$ meV), but still smaller than t_\perp . For example, if we consider $\alpha_1 \rightarrow \alpha_3$ hopping process in ABA stacked trilayer in Fig. 2, the valid range of magnetic field for the minimal model is given by

$$|\gamma_2| < \frac{(\hbar v / \ell)^2}{t_\perp} < t_\perp. \quad (3.24)$$

When γ_2 does not play an important role (in $N = 2$ stacks, for example), the lower limit of the validity range is parametrically smaller. The minimum field in bilayers has been estimated to be ~ 1 T,¹⁵⁾ by comparing intralayer hopping with the $\gamma_3 \sim 0.3$ eV interlayer hopping amplitude,

$$\hbar v_3 / l < \frac{(\hbar v / \ell)^2}{t_\perp} < t_\perp, \quad (3.25)$$

where $v_3 = (\sqrt{3}/2)a\gamma_3/\hbar$ and a is a lattice constant of graphene.

the odd-length chain zero-energy state and isolated states on the sublattice opposite to the chain ends. For a chain of length $2N - 1$, the chain's zero-energy state has nonzero amplitude on the N odd-index sites. The velocity is reduced from the single sheet velocity by a factor of $\sqrt{M/N}$, where M is the number of isolated sites opposite to the N odd-index sites. In a similar manner, higher J doublet Hamiltonians are sometimes altered by a multiplicative factor by perturbative coupling to smaller J doublets as in the single reversed layer example.

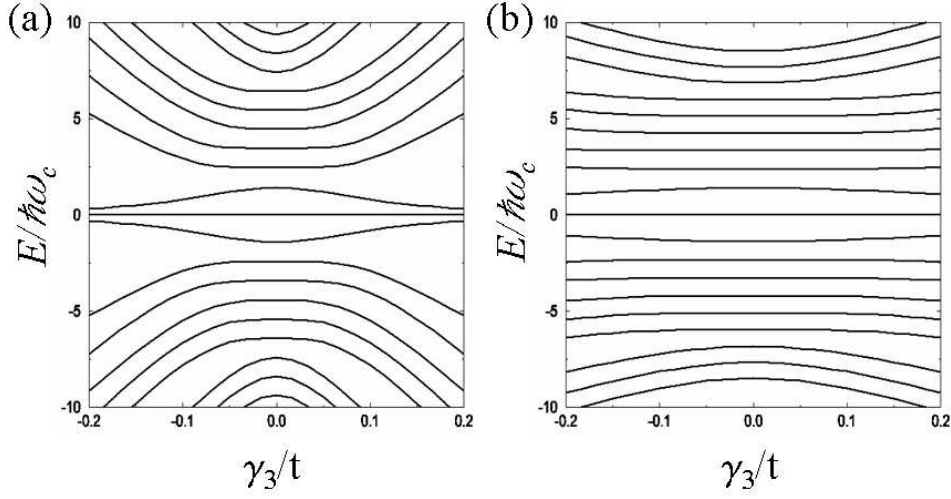


Fig. 11. Landau level spectrum near the K valley as a function of γ_3 for an AB stacked bilayer for (a) $B = 0.1$ T and (b) $B = 1$ T. Here $t = 3$ eV, $t_{\perp} = 0.1t$, and $\omega_c = eB/mc$, with $m = t_{\perp}/2v^2$, were used.

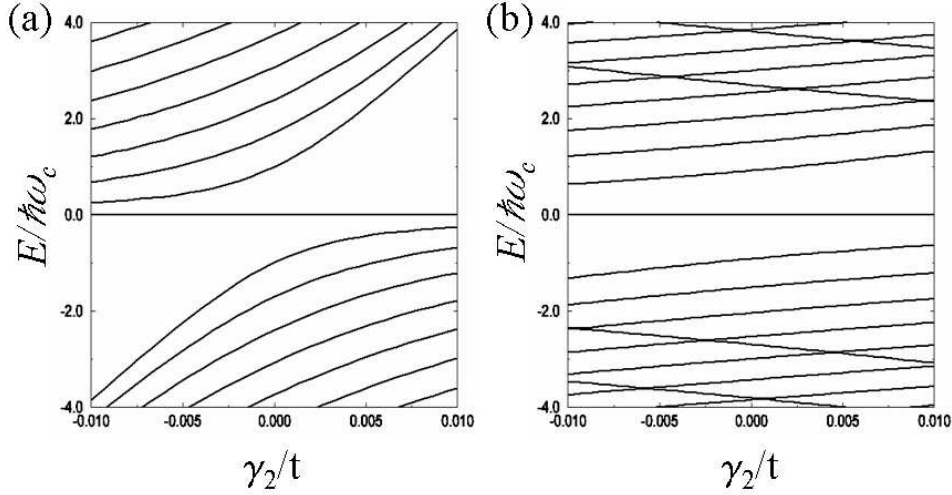


Fig. 12. Landau level spectrum near the K valley as a function of γ_2 for an ABA stacked trilayer for (a) $B = 1$ T and (b) $B = 10$ T. Here $t = 3$ eV, $t_{\perp} = 0.1t$, and $\omega_c = eB/mc$, with $m = t_{\perp}/2v^2$, were used. Note that for this case the Landau level structures near K and K' valleys are not identical.

Figures 11 and 12 show the Landau level spectrum at the K valley as a function of γ_3 for an AB stacked bilayer, and as a function of γ_2 for an ABA stacked trilayer, respectively. In the case of the bilayer, the dependence of the Landau levels on γ_3 is weak for B larger than 1 T, whereas in the case of the trilayer, the Landau level spectrum still strongly depends on γ_2 for $B = 1$ T, but the dependence becomes weak for B above 10 T, confirming the above argument.

3.3.2. Quantum Hall effect

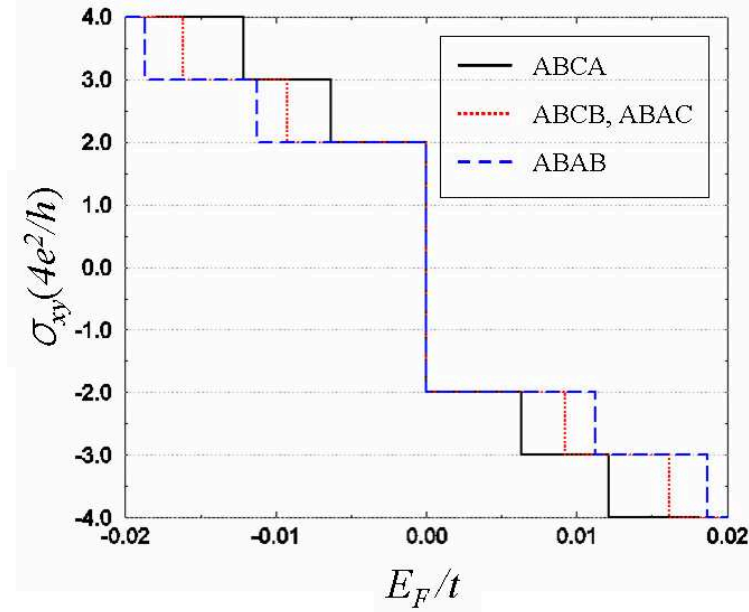


Fig. 13. (Color online) Noninteracting system Hall conductivity as a function of the Fermi energy for all inequivalent four-layer graphene stacks when $B = 10$ T, $t = 3$ eV, and $t_{\perp} = 0.1t$. The dependence of the Hall conductivity on Fermi energy is simply related to the dependence of the Hall conductivity on total electron density. The Hall conductivity calculations shown in this figure assume neutralizing ionized donors spread equally between the four layers.

In Fig. 13, we plot the noninteracting Hall conductivity as a function of Fermi energy for the four distinct four-layer stacks. When electron-electron interactions are included at an electrostatic mean-field (Hartree) level and the neutralizing ionized dopants (responsible for the Fermi energy shift away from the Dirac point) are assumed to be equally distributed among the layers, the Landau levels with $E \neq 0$ are shifted by electrostatic potential differences between the layers. There is, however, no influence of electrostatics on the $E = 0$ levels. This property follows from the perfect particle-hole symmetry of the models we employ, which implies a uniform charge distribution among the layers at the neutrality point. Remote (γ_2 2nd neighbor) interlayer hopping *does* shift the $E = 0$ Landau level in the ABAB stacked tetralayer and weakly lifts the degeneracy responsible for the large jump between the $\pm(4e^2/h)N/2$ Hall plateaus. This example demonstrates a tendency toward the grouping of N spin and valley degenerate Landau levels very close to $E = 0$ in general N -layer stacks even when remote neighbor hopping is included. Small gaps between these Landau levels are unlikely to lead to Hall plateaus unless disorder is very weak. When disorder is weak, on the other hand, electron-electron interaction effects beyond Hartree level are likely to be important and lead to strong quantum Hall effects at many filling factors, often ones associated with broken symmetries of different types.^{(20), (21), (22), (23), (24), (25)} The property that the Hall conductivity will tend to jump by four units on crossing the Dirac point for arbitrarily stacked tetralayer

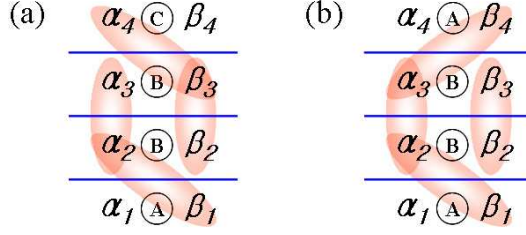


Fig. 14. (Color online) Stacking diagrams for tetralayer graphene with (a) ABBC stacking and (b) ABBA stacking. Shaded ovals link nearest interlayer neighbors.

graphene is the most obvious experimental manifestation of the chirality sum rule discussed in this paper. In practice charged multilayers ($E_F \neq 0$) would normally be prepared by placing the system on one side of an electrode and gating. Even though gating will redistribute charge and shift electric potentials differently in different layers, the Landau level bunching we discussed should still be clearly reflected in quantum Hall effect measurements.

3.3.3. Effects of the same stacking inside

The analysis presented so far is based on the assumption that stacking one layer directly on top of its neighbor, AA stacking, is not allowed. When interior AA stacking does occur, we can still apply a similar diagram analysis and identify the zero-energy states at the Dirac point. In this case, however, zero-energy states can appear not only at the Dirac points but also at other points in momentum space. The degenerate state perturbation theory at the Dirac point discussed so far therefore cannot completely capture the low-energy states.

As an example, let us consider ABBC stacked tetralayer graphene, as illustrated in Fig. 14(a). Here, in addition to α_1 and β_4 , there are two zero-energy states at each three-site-chain defined by

$$\begin{aligned} |\tilde{\beta}_1\rangle &= \frac{1}{\sqrt{2}} (|\beta_1\rangle - |\alpha_3\rangle), \\ |\tilde{\alpha}_4\rangle &= \frac{1}{\sqrt{2}} (|\alpha_4\rangle - |\beta_2\rangle). \end{aligned} \quad (3.26)$$

Thus the matrix elements between low-energy states are given by

$$\langle \alpha_1 | H | \tilde{\beta}_1 \rangle = \langle \tilde{\alpha}_4 | H | \beta_4 \rangle = -\frac{t_\perp}{\sqrt{2}} \nu^\dagger. \quad (3.27)$$

Therefore the system can be described by two massless Dirac modes with reduced velocity, as shown in Figs. 6(b) and 10(b).

Another example is ABBA stacked tetralayer graphene, as illustrated in Fig. 14.(b). In this case, there are two zero-energy states at α_1 and α_4 . The high-energy states Φ_r are given by Eq. (2.4) with $N = 4$, thus we get

$$\langle \alpha_1 | H | \alpha_4 \rangle = \sum_{r=1}^4 \frac{\langle \alpha_1 | V | \Phi_r \rangle \langle \Phi_r | V | \alpha_4 \rangle}{(-\epsilon_r)} = -ct_\perp |\nu|^2, \quad (3.28)$$

where $c = \frac{1}{5} \sum_r \sin\left(\frac{r\pi}{5}\right) \sin\left(\frac{4r\pi}{5}\right) / \cos\left(\frac{r\pi}{5}\right) = -1$. Here the low-energy state is composed of one *non-chiral* massive mode. Note that because of the non-chirality, there are no zero-energy Landau levels.

3.3.4. Pseudospin magnetism

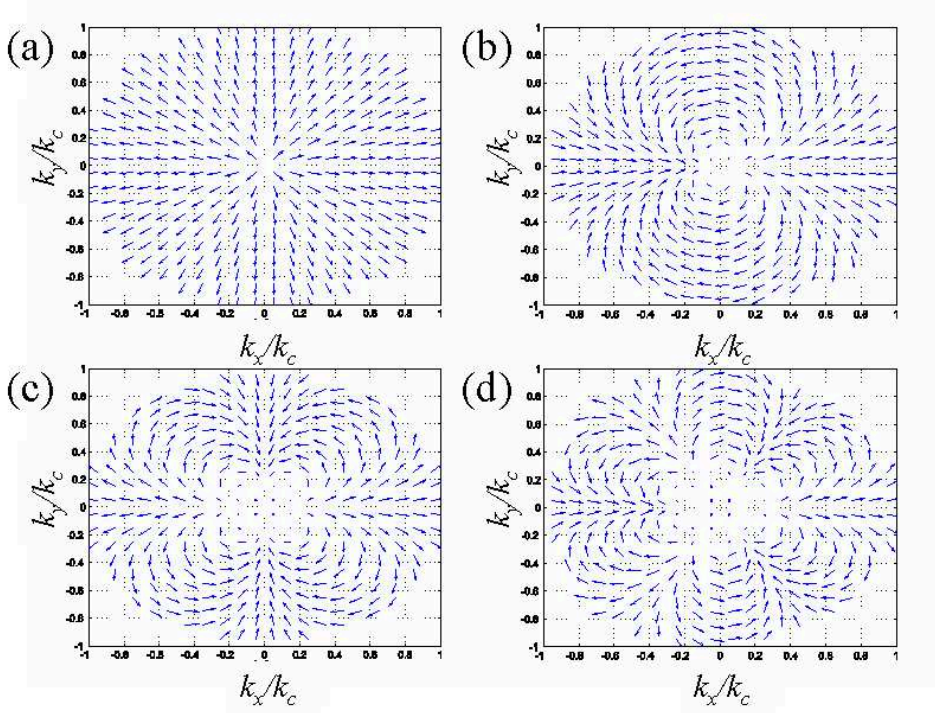


Fig. 15. (Color online) In-plane projected pseudospin orientation of (a) $J = 1$, (b) $J = 2$, (c) $J = 3$ and (d) $J = 4$ chiral 2D electron system for a neutral, unbiased system with coupling constant $\alpha \equiv e^2/\epsilon\hbar v = 1$ where ϵ is the dielectric constant. For $J > 1$, the arrows are shorter in the core of the momentum space vortex because the pseudospins in the core have rotated spontaneously toward \hat{z} or $-\hat{z}$ direction indicating the pseudospin magnetic state.

Finally, we note that in the presence of electron-electron interactions, chiral two-dimensional electron system (C2DES) tends toward momentum-space vortex states in which charge is spontaneously shifted between layers²⁶⁾ and that these instabilities are stronger in systems with larger J . Figure 15 shows in-plane projected pseudospin orientation for $J = 1, 2, 3, 4$ C2DESs, which correspond to $N = 1, 2, 3, 4$ ABC-stacked graphene multilayers. Note that for $J > 1$, the arrows in the core of the momentum space vortex have rotated spontaneously toward \hat{z} or $-\hat{z}$ direction indicating the spontaneous charge transfer between layers. The present work identifies ABC stacked multilayer graphene as the most likely candidate for this particular type of exotic broken symmetry state. Other types of broken symmetry might occur for other stacking sequences, especially in the quantum Hall regime.

§4. Conclusions

We have shown that N -layer graphene at intermediate and strong magnetic fields has a strong tendency towards the appearance of N spin and orbitally degenerate Landau levels very close to $E = 0$. This property should lead to strong quantum Hall effects at $\pm(4e^2/h)N/2$ in many N -layer stacks. The origin of this behavior is the following *chirality sum rule*: i) The low-energy bands of multilayer graphene can be decomposed into N_D doublets with chirality J_i . ii) Although N_D depends on the stacking sequence, $\sum_{i=1}^{N_D} J_i = N$ in an N -layer stack.

The chirality sum rule applies precisely only to idealized models with only nearest-neighbor intralayer and interlayer tunneling. It nevertheless suggests the likelihood of interesting interaction physics and broken symmetry ground states in many neutral or weakly doped multilayer graphene samples.

Acknowledgements

This work was supported by NSF-NRI SWAN and the Welch Foundation.

References

- 1) A. K. Geim and K. S. Novoselov, *Nature Materials* **6** (2007), 183.
- 2) A. K. Geim and A. H. MacDonald, *Phys. Today* **60** (8) (2007), 35.
- 3) K. S. Novoselov, A. K. Geim, S. V. Morozov, D. Jiang, Y. Zhang, S. V. Dubonos, I. V. Grigorieva, and A. A. Firsov, *Science* **306** (2004), 666.
- 4) C. Berger, Z. Song, T. Li, X. Li, A. Y. Ogbazghi, R. Feng, Z. Dai, A. N. Marchenkov, E. H. Conrad, P. N. First and W. A. de Heer, *Phys. Chem. B* **108** (2004), 19912.
- 5) T. Ohta, A. Bostwick, T. Seyller, K. Horn, and E. Rotenberg, *Science* **313** (2006), 951.
- 6) A. Rycerz, J. Tworzydł and C. W. J. Beenakker, *Nature Phys.* **3** (2007), 172.
- 7) V. V. Cheianov, V. Fal'ko and B. L. Altshuler, *Science* **315** (2007), 1252.
- 8) K. S. Novoselov, A. K. Geim, S.V. Morozov, D. Jiang, M. I. Katsnelson, I. V. Grigorieva, S. V. Dubonos and A. A. Firsov, *Nature* **438** (2005), 197.
- 9) Y. Zhang, Y. W. Tan, H. L. Stormer and P. Kim, *Nature* **438** (2005), 201.
- 10) The present article is an expanded version of Hongki Min and A. H. MacDonald, *Phys. Rev. B* **77** (2008), 155416.
- 11) J. Hass, F. Varchon, J. E. Millán-Otoya, M. Sprinkle, N. Sharma, W. A. de Heer, C. Berger, P. N. First, L. Magaud and E. H. Conrad, *Phys. Rev. Lett.* **100** (2008), 125504.
- 12) J. C. Charlier, J. P. Michenaud and X. Gonze, *Phys. Rev. B* **46** (1992), 4531.
- 13) P. D. Ritger and N. J. Rose, *Equations with Applications* (McGraw-Hill Book Company, New York, 1968).
- 14) F. Guinea, A. H. Castro Neto and N. M. R. Peres, *Phys. Rev. B* **73** (2006), 245426.
- 15) E. McCann and V. I. Fal'ko, *Phys. Rev. Lett.* **96** (2006), 086805.
- 16) J. J. Sakurai, *Modern Quantum Mechanics* (Addison Wesley, Reading, 1994).
- 17) M. Koshino and T. Ando, *Phys. Rev. B* **76** (2007), 085425.
- 18) J. L. Mañes, F. Guinea and M. A. H. Vozmediano, *Phys. Rev. B* **75** (2007), 155424.
- 19) M. Nakamura and L. Hirasawa, *Phys. Rev. B* **77** (2008), 045429.
- 20) D. A. Abanin, P. A. Lee and L. S. Levitov, *Phys. Rev. Lett.* **96** (2006), 176803.
- 21) K. Nomura and A. H. MacDonald, *Phys. Rev. Lett.* **96** (2006), 256602.
- 22) J. Alicea and M. P. A. Fisher, *Phys. Rev. B* **74** (2006), 075422.
- 23) M. O. Goerbig, R. Moessner and B. Douçot, *Phys. Rev. B* **74** (2006), 161407.
- 24) K. Yang, S. Das Sarma and A. H. MacDonald, *Phys. Rev. B* **74** (2006), 075423.
- 25) Y. Barlas, R. Cote, K. Nomura and A. H. MacDonald, *Phys. Rev. Lett.* **101** (2008), 097601.
- 26) Hongki Min, G. Borghi, M. Polini and A. H. MacDonald, *Phys. Rev. B* **77** (2008), 041407.